International Journal of Pharmaceutics 387 (2010) 172–179

Contents lists available at ScienceDirect

International Journal of Pharmaceutics

journal homepage: www.elsevier.com/locate/ijpharm

Analysis of nucleation kinetics of poorly water-soluble drugs in presence of ultrasound and hydroxypropyl methyl cellulose during antisolvent precipitation

Sameer V. Dalvi, Rajesh N. Dave*

Otto H. York Department of Chemical, Biological and Pharmaceutical Engineering, New Jersey Institute of Technology, Newark, NJ 07102, USA

ARTICLE INFO

Article history:
Received 25 August 2009
Received in revised form 6 December 2009
Accepted 10 December 2009
Available online 21 December 2009

Keywords:
Antisolvent
Ultrasound
Drug
Nucleation
Interfacial tension
Supersaturation

ABSTRACT

In this paper, nucleation kinetics of four poorly water-soluble drugs namely, itraconazole (ITZ), griseofulvin (GF), ibuprofen (IBP) and sulfamethoxazole (SFMZ) when precipitated by liquid antisolvent precipitation using water as antisolvent is examined in order to identify thermodynamic and kinetic process parameters as well as material properties that affect nucleation rate and hence, the particle size. The nucleation rates have been estimated for precipitation with and without ultrasound and hydroxypropyl methyl cellulose (HPMC). It is found that the nucleation rates increase significantly in presence of ultrasound and HPMC. Analysis of nucleation kinetics indicates that an increase in diffusivity due to ultrasound and a decrease in solid–liquid interfacial surface tension due to HPMC result in higher nucleation rates. Analysis also shows that reduction in interfacial surface tension due to HPMC is higher for a drug with lowest aqueous solubility (such as ITZ) as compared to drugs with higher aqueous solubility. It is also observed that it is easy to precipitate submicron particles of a drug with lowest aqueous solubility (such as ITZ) compared to drug molecules (such as SFMZ) with higher aqueous solubility in presence of HPMC.

1. Introduction

The bioavailability of poorly water-soluble hydrophobic drugs (Biopharmaceutics Classification System (BCS) Class II) is limited by their solubility and dissolution rate (Amidon et al., 1995; Lipinski, 2002). Many of new drugs are poorly water soluble (Lipinski, 2002), and their dissolution rate can be improved by decreasing particle size (Noyes and Whitney, 1897). Decrease in size increases the surface area which results in an increase in the rate of dissolution of these drugs in aqueous media of our body fluid (Liversidge and Cundy, 1995; Mosharraf and Nystorm, 1995). While there are many techniques available for size reduction, their applicability is limited because of poor control of particle size, morphology and scalability in comparison to liquid antisolvent (LAS) precipitation (Matteucci et al., 2006; Chen et al., 2006; Zhao et al., 2007). Therefore, in this work LAS precipitation technique is used to prepare aqueous suspensions of ultra-fine particles of four poorly water-soluble drugs, namely ITZ, GF, IBP and SFMZ.

Precipitation of a solid solute is achieved in LAS by increase in a molar volume of solution and hence a decrease in solvent power for solute by addition of a non-solvent (antisolvent) (Yeo and Lee, 2004). Precipitation process mainly involves, nucleation due to supersatuartion attained by mixing (Horn and Rieger, 2001; Myerson, 2002) and simultaneous growth of nuclei by coagulation and condensation (Matteucci et al., 2006; Ventosa et al., 2005). Higher nucleation rates result in low or negligible growth and hence can potentially produce submicron particles. Thus, in order to control the particle size, PSD, and improve the stability, it is necessary to increase nucleation rate, inhibit the particle growth and control agglomeration of particles by steric or electrostatic stabilization.

In this work, LAS precipitation has been carried out in presence of ultrasound to improve micromixing and HPMC to inhibit particle growth. Ultrasound generates the cycles of compression and rarefaction in the liquid medium, resulting in creation of tiny water vapor bubbles in the solution due to cavitation (Dennehy, 2003; Doktysz and Suslick, 1990; Prozorov et al., 2004). The bubbles ultimately collapse, and intense shock waves are generated and propagate through liquid at velocities higher than the speed of sound which imparts high velocities to the particles suspended in the solution (Doktysz and Suslick, 1990; Prozorov et al., 2004), leading to the uniform micromixing of solution and antisolvent. The sudden release of energy due to bubble explosion causes extremely rapid and localized temperature reduction in the solution to generate rapid nucleation in the solution. Recent literature (Amara et al., 2001; Nishida, 2004; Guo et al., 2005; Luque de Castro and Priego-Capote, 2007; Patil et al., 2008; Abbas et al., 2007) demonstrates the use of ultrasound, mainly for cooling crystallization, to reduce the particle size, size distribution and agglomeration of the particles.

* Corresponding author. Tel.: +1 973 596 5860; fax: +1 973 642 7088.
E-mail address: dave@njit.edu (R.N. Dave).

0378-5173/$ – see front matter © 2010 Elsevier B.V. All rights reserved.
doi:10.1016/j.ijpharm.2009.12.026

Nomenclature

A_{hom}	kinetic parameter in nucleation rate
B_{hom}	thermodynamic parameter in nucleation rate
C	concentration of API in the solution (mol/l)
C^*	equilibrium solid solubility in the aqueous solution (mol/l)
D_{AB}	the diffusion coefficient (m^2/s)
f	is the solute-free cosolvent volume fraction
J	nucleation rate (nuclei/m^3/s)
k	Boltzmann constant
K_{ow}	octanol–water partition coefficient
k_v	volume shape factor for the spherical particles
L_i	average size (μm)
ΔL_i	differential width of the size range i (μm)
M	universal constants related to solubility
M_T	final suspension density (g/cm^3)
N	universal Constants related to solubility
n_i	population density of particles (number/cm^3/μm)
N_A	Avogadro's number
r_0	radius of the molecule (cm)
S	supersaturation ratio
S_m	solubility in aqueous organic solution (mol/l)
S_w	water solubility (mol/l)
T	temperature (K)
Δ(wt%)	differential weight percent

Greek letters

ω	molecular volume (cm^3/molecule)
γ	surface tension (N/m)
γ_3	activity coefficient for solute
η	dynamic viscosity (cP)
σ	constant related to solubility
ρ_c	particle density (g/cm^3)

Abbreviations

AE	absolute errors
GF	griseofulvin
HPMC	hydroxypropyl methyl cellulose
IBP	ibuprofen
ITZ	itraconazole
LAS	liquid antisolvent
Polymer	JR400 hydroxyethylcellulose ethoxylate, quaternized
PVP	poly(vinylpyrrolidone)
PSD	particle size distribution
SD	standard deviation
SFMZ	sulfamethoxazole

The stability of precipitated particles in colloidal solution further depends on agglomeration or flocculation, driven by hydrophobic effects, electrostatic interaction as well as weak van der waals attractive forces. Deryagin-Landau-Verwey-Overbeek (DLVO) theory effectively describes such interactions and suggests steric and electrostatic stabilization as a way to improve the colloidal stability (Horn and Rieger, 2001; Napper, 1970). Cellulosic polymer such as HPMC has been shown to be the most effective growth inhibitor for precipitation GF particles in our previous work (Dalvi and Dave, 2009). HPMC being a neutral polymer offers steric stabilization to the particles in aqueous suspensions.

The purpose of this work therefore, is to study how addition of HPMC, presence of ultrasound and physico-chemical material properties can affect the nucleation rates and allow for manipulation of particle sizes. The nucleation rates have been estimated with and without HPMC and ultrasound using particle size distributions obtained by light scattering. The classical nucleation theory for homogeneous nucleation has been used to analyze the influence of ultrasound and HPMC as well as aqueous solubility of APIs (and hence supersaturation) on the nucleation rates.

2. Theory

2.1. Nucleation kinetics

According to the classical theory of homogeneous nucleation (Lindenberg and Mazzotti, 2009), nucleation rate (J) is given as:

$$J = A_{hom} S \exp\left(-\frac{B_{hom}}{\ln^2 S}\right) \quad (1)$$

where A_{hom} is a kinetic parameter and B_{hom} is a thermodynamic parameter.

A_{hom} depends on the mechanisms of attachment (Lindenberg and Mazzotti, 2009), namely interface-transfer control and volume diffusion control. According to Lindenberg and Mazzotti (2009), volume diffusion control never applies to the new nuclei formed in the solution in the early phase of growth as diffusion is infinitely fast for such particles. Therefore, it is assumed in this work that for nucleation step, the main mechanism of attachment is the interface-transfer controlled. A_{hom} for interface-transfer control is given as (Lindenberg and Mazzotti, 2009),

$$A_{hom} = \left(\frac{4\pi}{3\omega}\right)^{1/3} \left(\frac{\gamma}{kT}\right)^{1/2} D_{AB} C^* N_A \quad (2)$$

and B_{hom} is defined as follows:

$$B_{hom} = \frac{16\pi\omega^2\gamma^3}{3(kT)^3} \quad (3)$$

D_{AB}, the diffusion coefficient is given by Stokes–Einstein equation:

$$D_{AB} = \frac{kT}{6\pi r_0 \eta}. \quad (4)$$

where r_0 is the radius of the molecule, η is the dynamic viscosity of the solution, ω is the molecular volume, C^* is the equilibrium solid solubility in the aqueous solution, S is the degree of supersaturation, γ is the surface tension at the solid–liquid interface, k is the Boltzmann constant, N_A is the Avogadro's number, and T is the solution temperature.

3. Experimental

3.1. Materials

ITZ was purchased from Hawkins Inc., USA. GF was as a gift received from Johnson and Johnson Co. Ltd., USA. IBP (grade 110) was purchased from Alfa Chem, USA. SFMZ was purchased from MP Biomedicals, L.L.C, USA. Acetone (99.8% pure), tetrahydrofuran (THF) (anhydrous, ≥99.9% pure) and hydroxypropyl methyl cellulose (HPMC) (3500–5600 cPs) were purchased from Sigma–Aldrich Inc., USA. All these chemicals were used without further purification. Deionized Millipore water was used as an antisolvent.

3.2. Apparatus and experimental procedure

Organic solution of API in organic solvent (50–200 mg/ml) is introduced in water (200 ml) containing 0.2 wt% HPMC, maintained at a constant temperature (1 °C) through a stainless steel nozzle (0.01 in. i.d.) at a flow rate of 100 ml/min using HPLC pump (by Lab Alliance, USA). The ultrasound horn is immersed in the antisolvent at an immersion depth (below the antisolvent level) of 1.5 in. The

tip ((1/2) in. i.d.) of an ultrasound horn (Omni-ruptor 250 by Omni International Inc., USA) is directed over a nozzle such that the flow of the solution is dispersed instantaneously in antisolvent by the vibrating (75 W operating at frequency of 20 kHz) surface of the tip. Detailed description of the experimental apparatus can be found in our previous work (Dalvi and Dave, 2009). The solution is insonated for the time till the addition of solution in antisolvent is complete. Aqueous suspension of API particles (~5 mg/ml) thus obtained is then analyzed for particle size and distribution by laser scattering (Beckman Coulter LS 230). Field Emission Scanning Electron Microscope (LEO 1530VP FE-SEM) is used to observe the surface morphology of the precipitated GF particles. XRD (Phillips X'pert MRD Diffractometer) and DSC (FP84 Mettler-Toledo K.K.) have been used to compare the physical characteristics of APIs before and after processing.

4. Data treatment

4.1. Estimation of supersaturation

Mixing of organic solution of API with water lowers API solubility in a mixture of organic solvent due to increase in molar volume. Supersaturation, thus generated leads to nucleation and precipitation. According to Eq. (1), nucleation rate is directly proportional to the supersaturation. Therefore it is necessary to estimate the supersaturation generated after mixing of antisolvent and solution streams. Supersaturation is defined as,

$$S = \frac{C}{C^*} \tag{5}$$

where C is the actual concentration of API in the solution (mol/L) and C^* is the equilibrium solubility (mol/L) of API in a mixture of organic solvent and water. Therefore, in order to estimate the supersaturation generated after mixing, it is necessary to estimate C^* at the solution temperature and organic solvent content of the aqueous mixture in presence of stabilizers.

It is possible that the use of stabilizers may change the solubility of APIs in the solution (Loftsson et al., 1996). However, for three APIs (ITZ, IBP and SFMZ) studied in this work, HPMC has negligible effect on the aqueous solubility as reported in the literature. Matteucci et al. (2007) show that the increase in ITZ solubility in presence of HPMC at 500-fold higher concentration (than that of ITZ) is negligible. Note that the level of HPMC used in this work is 0.2% (w/v), which is 0.4 times the amount of ITZ used in this work. Patent WO 98/19708 filed by Donabedian et al. (1996) (Union Carbide Chemicals and Plastic Technology Corporation) presents data showing negligible increase in IBP solubility in presence of 1 and 2% (w/v) HPMC. Irevolino et al. (2000) also show that HPMC does not affect aqueous solubility of IBP. Again, the level of HPMC used in this work is 0.2% (w/v) is relatively low. Also, Loftsson et al. (1996) show that the use of HPMC does not significantly increase solubility of SFMZ in water at a pH range of 3–6. A pH condition of 4.3 in presence of 0.2 wt% HPMC was obtained in this work for SFMZ precipitation (as shown in Table 4), which is in the range reported in Loftsson et al. (1996). Therefore, it is justifiable to assume that HPMC does not significantly change solubility of GF in water as its aqueous solubility mainly lies in the range covered by ITZ, IBP and SFMZ. However, in absence of any literature data, aqueous solubility of GF in presence of HPMC was estimated experimentally using UV–VIS spectrophotometer. An excess of GF was added in deionized water containing 0.2 wt% HPMC and was stirred overnight at 20 °C. The known amount of sample was filtered through a 0.2 μm syringe filter, and analyzed by Agilent UV–VIS spectrophotometer (Santa Clara, CA) using an absorption wavelength of 296 nm to detect GF. As expected, it was found that GF solubility nominally increases by 4% in presence of HPMC and is reported in Table 1.

Also, experiments in this work were carried out at 1 °C in presence of organic solvents and hence the effect of organic solvent and lower temperature of 1 °C on the solubilities can be significant. In order to determine the solubility of GF, IBP and SFMZ in mixture of water and acetone at 1 °C, a correlation proposed by Li and Yalkowsky (1998) was used to predict the effect of organic solvent on the aqueous solubility of APIs at 20 °C. Similarly, solubility of ITZ in water (S_w) and water and THF mixture (S_m) (for given composition of THF and water) at 20 °C was used as reported by Kumar et al. (2009) The effect of temperature on solubility was then estimated using solid–liquid phase equilibrium calculations.

4.1.1. Drug solubility in aqueous organic solutions at 20 °C

The API solubility in water–organic solvent mixture (S_m) was estimated using the following log-linear model proposed by Li and Yalkowsky (1998).

$$\log S_m = \log S_w + f\sigma \tag{6}$$

where S_w is the water solubility and f is the solute-free cosolvent volume fraction.

σ was predicted using the octanol–water partition coefficient, K_{ow} as per the following equation:

$$\sigma = M \log K_{ow} + N \tag{7}$$

As suggested by Li and Yalkowsky (1998), the values of M and N are universal as they depend on solvent polarity. For acetone, which is the organic solvent used in this work for GF, IBP and SFMZ (except ITZ), values of M and N used are 1.14 and −0.10 respectively for drug molecules with $\log K_{ow}$ ranging from −1.38 to −5.66 (Li and Yalkowsky, 1998).

Solubility of ITZ in water (S_w) and water and THF mixture (S_m) (for given composition of THF and water) at 20 °C was used as reported by Kumar et al. (2009) and σ was then estimated. σ, thus estimated was then used to determine solubility of ITZ in water and THF mixture (S_m) (for given composition of THF and water in this work) at 20 °C.

4.1.2. Effect of temperature on drug solubility in aqueous organic solution

In order to estimate the effect of temperature on the solubility, activity coefficients for ITZ, GF, IBP and SFMZ at 20 °C were first

Table 1
Physico-chemical properties and solubilities of API molecules in water and aqueous organic mixtures at 20 and 1 °C.

API	T_m (°C)	ΔH^f (J/g)	$\log K_{ow}$ at 20 °C	S_w (mg/L) at 20 °C	S_m (mg/L) at 20 °C	S_m (mg/L) at 1 °C	$\ln S$ at 1 °C
ITZ	166.2	85	5.66	0.000472	0.10[a]	0.00837	13.2
GF	220	132.4	2.18	8.99	15.44[b]	2.66	7.5
IBP	76	125	3.97	21	34.87[c]	7.834	6.4
SFMZ	167	133.63	0.89	610	649.40[d]	171.584	3.3

[a] 9.1 vol.% of THF in water–solvent mixture.
[b] 9.1 vol.% of acetone in water–solvent mixture.
[c] 4.8 vol.% of acetone in water–solvent mixture.
[d] 2.4 vol.% of acetone in water–solvent mixture.

calculated using Eq. (8) and physico-chemical properties such as melting point and heat of fusion (reported in Table 1).

$$\gamma_3 = \frac{1}{x_3}\exp\left\{\frac{\Delta H_m}{R}\left(\frac{1}{T_m} - \frac{1}{T}\right)\right\} \quad (8)$$

According to regular solution theory (Prausnitz et al., 1999), activity coefficient is inversely proportional to the temperature. Thus, effect of temperature on activity coefficient was estimated using Eq. (9) and then solubility at 1 °C was then estimated using Eq. (8).

$$\ln \gamma_3 = \frac{A(T)}{T} \quad (9)$$

4.2. Nucleation rate determination

To estimate nucleation rates, the particle number distribution data obtained from light scattering, were converted to a cumulative mass percent distribution and then the values of population densities were calculated using the following equation (Jarmer et al., 2004):

$$n_i = \frac{\Delta(\text{wt}\%)M_T}{k_v \rho_c L_i^3 \Delta L_i} \quad (10)$$

where n_i is the population density of particles with average size L_i. Δ(wt%) and ΔL_i are the differential weight percent and the width of the size range i, respectively. k_v is the volume shape factor for the spherical particles. M_T and ρ_c are final suspension density and the particle density respectively.

Nucleation rate was determined using Eq. (11) (Zarkadas and Sirkar, 2006) as MSMPR model does not fit well to the population densities calculated (as can be seen from Figs. 1 and 2).

$$J = \frac{\int_{L_i}^{L_{i+1}} n_i(L_i)\, dL_i}{t_{samp}} \quad (11)$$

5. Results and discussions

5.1. Drug solubility and supersaturation

Table 1 presents solubilities of API molecules in water and aqueous organic mixtures at 20 and 1 °C and the supersaturation (ln S) attained after mixing organic solutions with water at 1 °C. It can be seen that ITZ is the least water-soluble API whereas SFMZ is the highly soluble among the list presented in Table 1. Therefore, the supersaturation attained after mixing antisolvent and organic solution is highest (13.2 at 1 °C) for ITZ and is lowest (3.3 at 1 °C) for SFMZ.

5.2. Effect of ultrasound on LAS precipitation

Tables 2 and 3 present the details of size and size distribution of API particles precipitated by LAS without and with ultrasound respectively. Table 5 presents the nucleation rates calculated for the precipitation without and with ultrasound. It can be seen that the use of ultrasound increases the nucleation rates and hence particle size decreases.

Table 2
Size and size distribution of API particles precipitated by introducing organic solutions of APIs through 0.01 in. i.d. nozzle at 100 ml/min in 200 ml water maintained at 1 °C.

API	PS	SD	D10/D50/D90	% < 1 μm
ITZ[a]	19.6	9.4	9.6/18.24/30.0	0
GF[b]	24.4	16.7	7.1/20.0/51.2	0
IBP[c]	68.9	47.7	16.5/58.3/146.0	0
SFMZ[d]	32.5	20.0	10.2/27.5/62.8	0

[a] 50 mg/ml in THF.
[b] 50 mg/ml in acetone.
[c] 100 mg/ml in acetone.
[d] 200 mg/ml in acetone.

Table 3
Size and size distribution of API particles precipitated by introducing organic solutions of APIs through 0.01 in. i.d. nozzle at 100 ml/min in 200 ml water maintained at 1 °C and 75 W sonication through 0.5 in. probe.

API	PS	SD	D10/D50/D90	% < 1 μm
ITZ[a]	20.6	9.48	9.4/19.5/33.1	0
GF[b]	5.4	2.776	2.1/5.0/9.4	0.2
IBP[c]	30.5	18.99	11.3/25.7/60.5	0
SFMZ[d]	15.6	8.86	4.3/15.1/28.4	0

[a] 50 mg/ml in THF.
[b] 50 mg/ml in acetone.
[c] 100 mg/ml in acetone.
[d] 200 mg/ml in acetone.

Table 4
Size and size distribution of API particles precipitated by introducing organic solutions of APIs through 0.01 in. i.d. nozzle at 100 ml/min in 200 ml water (with 0.2 wt% HMPC dissolved and) maintained at 1 °C with 75 W sonication through 0.5 in. probe.

API	PS	SD	D10/D50/D90	% < 1 μm	pH after particle formation
ITZ[a]	0.83	0.6	0.2/0.5/1.9	68	5.4
GF[b]	2.4	1.0	1.6/2.0/4.2	0	5
IBP[c]	8.4	5.8	2.8/6.3/18.2	0	4.2
SFMZ[d]	30	17.7	8.6/26.7/56.6	0	4.3

[a] 50 mg/ml in THF.
[b] 50 mg/ml in acetone.
[c] 100 mg/ml in acetone.
[d] 200 mg/ml in acetone.

Nucleation rates mainly depend on supersaturation and interfacial energy (γ). Ultrasound, however, have been shown to not to affect equilibrium solubility as well as γ (Guo et al., 2005). Therefore, ultrasound does not affect the term, $(-(B_{hom}/\ln^2 S))$ in Eq. (1) which also means that an increase in nucleation rate is because of an increase in the value of A_{hom} with the use of ultrasound. A_{hom} mainly depends on D_{AB} and as shown in Table 5, ultrasound increases D_{AB} by many folds and hence results in increase in nucleation rate. Table 6 reports the enhancement (E_{DAB}) in D_{AB} as calculated using Eqs. (1)–(3). Similar observation was made by Guo et al. (2005) and it was observed that the use of ultrasound for LAS precipitation of roxithromycin increases D_{AB} by 3.82-fold.

5.3. Effect of HPMC on LAS precipitation

Table 4 presents details of size and size distribution of API particles precipitated by LAS in presence of HPMC and ultrasound. It can be seen that the particle size has been considerably reduced as compared to the case when no ultrasound and no HPMC was used. The nucleation rates presented in Table 5 suggest that the use of HPMC in addition to ultrasound tremendously increase the nucleation rates as compared to the case when no HPMC or ultrasound was used or when only ultrasound was used.

Table 5
Effect of ultrasound and HPMC on nucleation rates.

API	J (1/m^3 S) No ultrasound No HPMC	J (1/m^3 S) Ultrasound No HPMC	J (1/m^3 S) Ultrasound HPMC
ITZ	2.55×10^{13}	3.56×10^{13}	3.85×10^{18}
GF	7.91×10^{13}	2.66×10^{15}	9.23×10^{15}
IBP	6.96×10^{13}	1.26×10^{14}	1.15×10^{15}
SFMZ	9.21×10^{13}	7.27×10^{14}	1.40×10^{14}

Table 6
Effect of ultrasound and HPMC on diffusivity.

API	D_{AB} ($\times 10^{10}$ m^2/s) No ultrasound No HPMC	D_{AB} ($\times 10^{10}$ m^2/s) Ultrasound No HPMC	E_{DAB}[a]	D_{AB} ($\times 10^{10}$ m^2/s) Ultrasound HPMC
ITZ	1.42	1.98	1.4	0.48
GF	1.61	54.1	33.6	13.0
IBP	1.95	3.54	1.82	0.85
SFMZ	1.64	12.9	7.9	3.1

[a] Only due to ultrasound.

Table 7
Effect of HPMC on interfacial surface tension.

API	γ (mJ/m^2)	γ (Eq. (13)) (mJ/m^2)	γ^a (mJ/m^2)	$\Delta\gamma^a$ (%)	n^*
ITZ	43.97	45.86	39.34	−10.5	5
GF	39.1	41.23	38.31	−2.0	12
IBP	51.90	55.2	50.53	−2.6	14
SFMZ	23.61	28.39	23.65	0.15	28

[a] Changed due to HPMC.

Analysis of nucleation rates using classical nucleation theory suggests that nucleation rates change as the values of γ and D_{AB} change with the addition of HPMC. Tables 6 and 7 present the changes in D_{AB} and γ respectively, due to addition of HPMC. Addition of HPMC (0.2 wt%) in water increases the kinematic viscosity of water from 1.728 to 7.201 mm^2/s at 1 °C. Increase in viscosity decreases D_{AB} as estimated by Eq. (4). Thus values of D_{AB} decrease with addition of HPMC as compared to the case when only ultrasound was used as shown in Table 6.

Table 7 also presents the values of number of molecules forming the critical nucleus (n^*). Values of n^* were calculated using following equation (Roelands et al., 2006):

$$n^* = \frac{32\pi\omega^2\gamma^3}{3(kT)^3\ \ln^3 S} = \frac{2B_{\text{hom}}}{\ln^3 S} \tag{12}$$

Classical nucleation theory assumes that density and interfacial energy of nuclei can be described by the corresponding values of macroscopic crystals. However, as the number of nuclei forming molecules (n^*) decreases to 1 this assumption is no longer valid and classical nucleation pathway ceases to be applicable (Horn and Rieger, 2001; Lindenberg and Mazzotti, 2009; Basios et al., 2009). The values of n^* reported in Table 7 range from 5 to 28 which are relatively far away from the $n^* \to 1$ limit. Therefore, the application of classical nucleation theory for precipitation of all the APIs studied here is valid as $n^* > 1$, noting that the n^* value reported in (Lindenberg and Mazzotti, 2009) was as low as 4.

According to Eqs. (1)–(3), the nucleation rate is directly proportional to supersaturation and inversely proportional to the interfacial energy (γ). Since addition HPMC is unlikely to change the equilibrium solubilities of APIs (as explained earlier in Section 4.1) and hence the supersaturations attained, it is clear that change in γ in presence of HPMC alters the nucleation rates. Values of γ were estimated from nucleation rate determined using population densities. Eqs. (1)–(3) were solved for γ for precipitation with and without HPMC. Values of γ were also predicted using a correlation (Eq. (13)) suggested by Mersmann (1999) in order to compare the values of γ obtained from nucleation rates.

$$\gamma = 0.414KT\left(\frac{N_A}{\upsilon}\right)^{2/3} \ln\left[\frac{1}{\upsilon C^*}\right] \tag{13}$$

Table 3 presents values of γ calculated from Eq. (13). It can be seen that the predicted values are higher than the values calculated from nucleation rates and % absolute errors (%AE) vary for all the APIs. %AE for ITZ, GF, IBP and SFMZ are 4.1, 5.1, 6.0, and 16.8 respectively.

Comparison of γ values with (presented in Table 7) and without HPMC (presented in Table 3) show that HPMC reduces γ due to adsorption at the growing solid–liquid interfaces. One more interesting observation that can be made is that % change in γ is higher for API with least water solubility (such as ITZ) than API with higher water solubility (such as SFMZ).

HPMC was found to be the most efficient growth inhibitor for LAS precipitation of GFas compared to PVP and Polymer JR 400 (Dalvi and Dave, 2009). This is mainly because HPMC is more hydrophobic and has least solubility in water. It can interact strongly with more hydrophobic API such as ITZ whereas it cannot

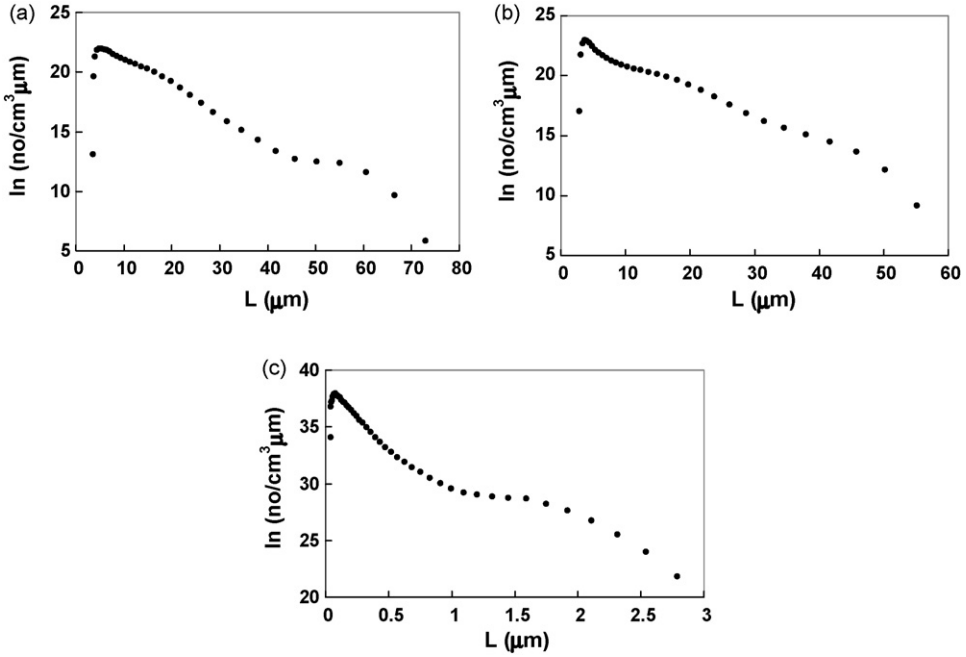

Fig. 1. Population density plots for antisolvent crystallization ITZ from its organic solutions in THF (5 mg/ml) introduced through 0.01 in. i.d. nozzle at 100 ml/min in 200 ml water as antisolvent at 1 °C (a) without ultrasound and HPMC, (b) with ultrasound (75 W) and no HPMC, and (c) with ultrasound (75 W) and with HPMC (0.2 wt% in water).

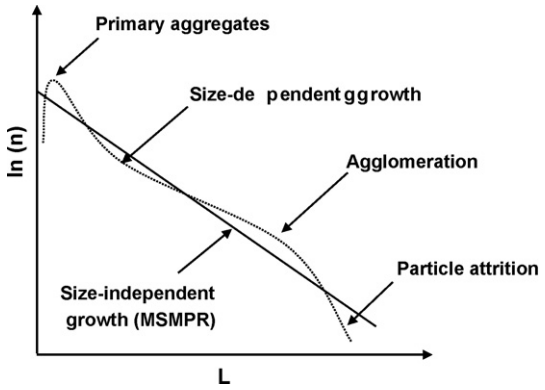

Fig. 2. Schematic of population density plot showing deviations from MSMPR.

interact favorably with API such as SFMZ as it is more hydrophilic and has more water solubility. Therefore, HPMC adsorption at growing interface of ITZ in the solution is more and hence the reduction in surface tension is higher as compared to SFMZ. Addition of HPMC results in a slight increase in surface tension at SFMZ–solution interface which indicates that HPMC does not adsorb at the SFMZ–solution interface. This increases agglomeration of the particles and hence larger particle sizes are obtained.

5.4. Characterization of particles

Fig. 3 shows SEM images of ITZ, GF and SFMZ particles precipitated by LAS. ITZ particles were mainly spherical whereas GF and SFMZ mainly show bipyramidal and diamond shaped morphology. It is also evident that from the surface morphology of GF (Fig. 3d) and SFMZ (Fig. 3f) that the growth of particles is mainly layer by layer and by diffusion control (Dirksen and Ring, 1991). The adsorption of HPMC at the solid–liquid interface prevents transfer of solute from the solution to the interface and hence results in uneven growth of the surface. Adsorption of HPMC on the surface forms net-like structure and hence solute molecule can only be deposited on the vacant sites forming finger like protrusions (Dalvi and Dave, 2009; Raghavan et al., 2001).

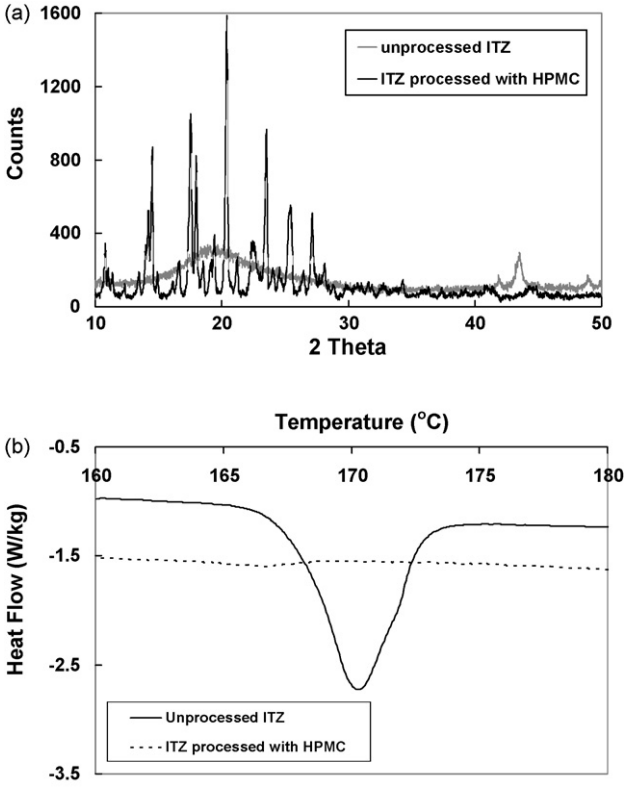

Fig. 4. (a) XRD pattern for unprocessed ITZ and ITZ processed with HPMC and (b) DSC curves for unprocessed ITZ and ITZ processed with HPMC.

Figs. 4–7 present XRD patterns and DSC curves for APIs unprocessed and processed with HPMC. XRD patterns for ITZ (Fig. 4a) show high amorphous characteristics which are also confirmed by DSC curves for processed and unprocessed ITZ (Fig. 4b). While there is a sharp peak for the melting of unprocessed ITZ, there is no distinct peak for ITZ processed with HPMC. The melting point of unprocessed ITZ was found to be ~168 °C whereas the phase transition temperature for ITZ processed with HPMC was found to be ~164 °C. XRD patterns for GF (Fig. 5a), IBP (Fig. 6a) and SFMZ

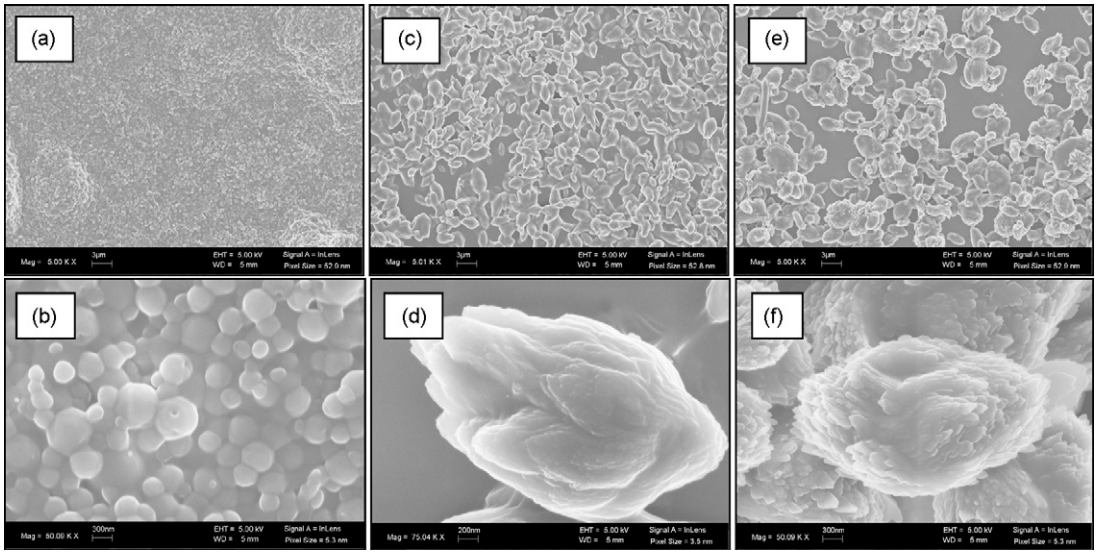

Fig. 3. SEM images of API particles precipitated by LAS from their organic solutions introduced through 0.01 in. i.d. nozzle at 100 ml/min in 200 ml water as antisolvent at 1 °C with ultrasound (75 W) and with HPMC (0.2 wt% in water): ITZ particles precipitated from THF (50 mg/ml) (a) 5000× and (b) 50,000×, GF particles precipitated from acetone (50 mg/ml) (c) 5000× and (d) 75,000× and SFMZ particles precipitated from acetone (200 mg/ml) (e) 5000× and (f) 50,000×.

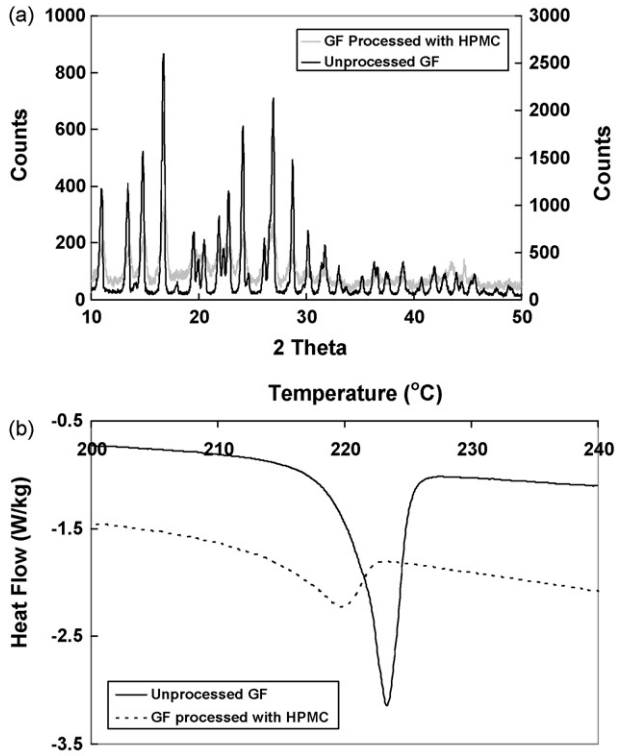

Fig. 5. (a) XRD pattern for unprocessed GF and GF processed with HPMC and (b) DSC curves for unprocessed GF and GF processed with HPMC.

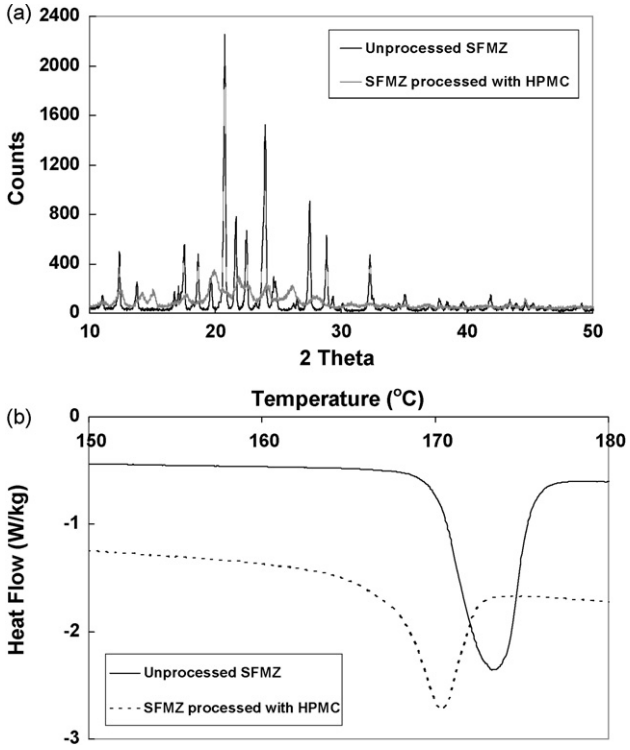

Fig. 7. (a) XRD pattern for unprocessed SFMZ and SFMZ processed with HPMC and (b) DSC curves for unprocessed SFMZ and SFMZ processed with HPMC.

(Fig. 7a) show reduction in peak intensities mainly confirming the size reduction or reduction in crystallinity. DSC curves (Figs. 5b–7b) for unprocessed GF, IBP and SFMZ indicate the melting points of 220, 76 and 170 °C whereas DSC curves of processed FNB, GF, IBP and SFMZ indicate the phase transition temperatures of 215, 68 and 168 °C.

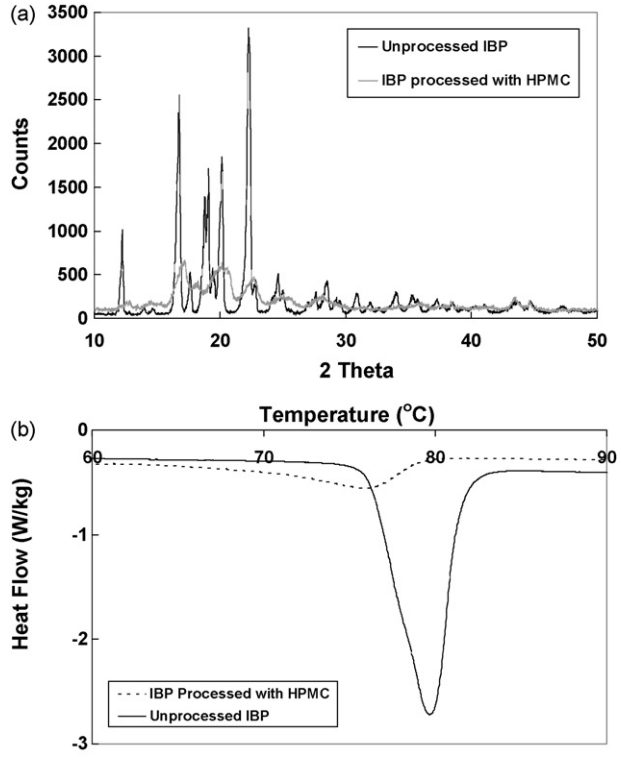

Fig. 6. (a) XRD pattern for unprocessed IBP and IBP processed with HPMC and (b) DSC curves for unprocessed IBP and IBP processed with HPMC.

6. Conclusions

Influence of HPMC, ultrasound and physico-chemical material properties on the nucleation rates and subsequently on particle sizes is examined based on four poorly water-soluble drugs through the LAS precipitation. The nucleation rates were estimated using population densities calculated from particle size distribution data. The nucleation rate data thus obtained, shows that nucleation rates increase in presence of ultrasound and HPMC. Use of ultrasound increases diffusivity of API molecules in the solution, increases A_{hom} and thus contribute to the increase in nucleation rate. Addition of HPMC also increases the viscosity of the solution and decreases the diffusivity and thus decreases A_{hom}. However, addition of HPMC decreases solid–liquid interfacial surface tension, and decreases B_{hom}. Thus, use of HPMC reduces the energy barrier for nucleation and increases the nucleation rate. Also it is observed that the decrease in the energy barrier of nucleation due to HPMC is higher for more hydrophobic molecule such as ITZ as compared to a moderately hydrophilic molecule such as SFMZ. This is because % reduction in surface tension is higher for ITZ than for SFMZ as HPMC interact favorably with hydrophobic molecule such as ITZ, whereas it does not interact and hence does not get adsorbed at the SFMZ particle interface and hence no reduction in interfacial energy. Also, it is found that the supersaturation attained after mixing is high for a more hydrophobic molecule such as ITZ as compared to a moderately water-soluble molecule of SFMZ. This is because hydrophobic molecule such as ITZ has very low equilibrium solubility in antisolvent–solvent mixture as compared to a moderately hydrophilic molecule such as SFMZ. Therefore, the nucleation rates obtained for ITZ are always higher than those obtained for SFMZ. The analysis of nucleation presented in this work indicates that the particle size of poorly water-soluble drugs precipitated by

LAS mainly depends material properties such as aqueous solid solubility and interfacial surface tension. Therefore, a better control over the particle size and size distribution can be achieved through is a careful manipulation of process parameters and material properties.

Acknowledgements

The authors gratefully acknowledge the financial support from the National Science Foundation (NSF) through grant #EEC-0540855. Authors would also like to thank Christian Beck for his help with estimation of GF solubility using UV–VIS spectrophotometer.

References

Abbas, A., Srour, M., Tang, P., Chiou, H., Chan, H., Romagnoli, J., 2007. Sonocrystallization of sodium chloride particles for inhalation. Chem. Eng. Sci. 62, 2445–2453.
Amara, N., Ratsimba, B., Wilhelm, A., Delmas, H., 2001. Crystallization of potash alum. Ultrason. Sonochem. 8, 265–270.
Amidon, G., Lennernas, H., Shah, V., Crison, J., 1995. A theoretical basis for a biopharmaceutical drug classification: the correlation of in vitro drug product dissolution and in vivo bioavailability. Pharm. Res. 12, 413–420.
Basios, V., Lutsko, J., Nicolis, G., Maes, D., Kirschhock, C., 2009. A new paradigm of crystallization arising from non-standard nucleation pathways. Microgravity Sci. Technol. 21, 47–51.
Chen, J., Zhang, J., Shen, Z., Zhong, J., Yun, J., 2006. Preparation and characterization of amrphous cefuroxime axetil drug nanoparticles with novel technology: high-gravity antisolvent precipitation. Ind. Eng. Chem. Res. 45, 8723–8727.
Dalvi, S.V., Dave, R.N., 2009. Controlling particle size of poorly water soluble drug using ultrasound and stabilizers in antisolvent precipitation. Ind. Eng. Chem. Res. 48, 7581–7593.
Dennehy, R., 2003. Particle engineering using power ultrasound. Org. Proc. Res. Dev. 7, 1002–1006.
Dirksen, J., Ring, T., 1991. Fundamentals of crystallization: kinetic effects on particle size distributions and morphology. Chem. Eng. Sci. 46, 2389–2427.
Doktysz, S., Suslick, K., 1990. Interparticle collisions driven by ultrasound. Science 247, 1067–1069.
Donabedian, D.H., Lawrence, M., Clark, E., 1996, Method for enhancing the solubility of substantially water-soluble compounds. PCT Patent No. WO 98/19708, 4 November.
Guo, Z., Zhang, M., Li, H., Wang, J., Kougoulos, E., 2005. Effect of ultrasound on antisolvent crystallization process. J. Crystal Growth 273, 555–563.
Horn, D., Rieger, J., 2001. Organic nanoparticles in the aqueous phase-theory, experiment, and use. Angew. Chem. Int. Ed. 40, 4330–4361.
Irevolino, M., Raghavan, S., Hadgraft, J., 2000. Membrane penetration enhancement of ibuprofen using supersaturation. Int. J. Pharm. 198, 229–238.
Jarmer, D., Lengsfeld, C., Randolph, T., 2004. Nucleation and growth rates of poly(L-lactic acid) microparticles during precipitation with a compressed-fluid antisolvent. Langmuir 20, 7254–7264.
Kumar, V., Wang, L., Riebe, M., Tung, H., Prudhomme, R., 2009. Formulation and stability of itraconazole and odanacatib nanoparticles: governing physical parameters. Mol. Pharm. 6, 1118–1124.
Li, A., Yalkowsky, S., 1998. Predicting cosolvency. 1. Solubility ratio and solute log *K*. Ind. Eng. Chem. Res. 37, 4470–4475.
Lindenberg, C., Mazzotti, M., 2009. Effect of temperature on the nucleation kinetics of α L-glutamic acid. J. Crystal Growth 311, 1178–1184.
Lipinski, C., 2002. Poor aqueous solubility—an industry wide problem in drug discovery. Am. Pharm. Rev. 53, 82–85.
Liversidge, G., Cundy, K., 1995. Particle size reduction for improvement of oral bioavailability of hydrophobic drugs: absolute oral bioavailability of nanocrystalline Danzol in beagle dogs. Int. J. Pharm. 125, 91–97.
Loftsson, T., Fridriksdottir, H., Gudmundsdottir, T.K., 1996. The effect of water-soluble polymers on aqueous solubility of drugs. Int. J. Pharm. 127, 293–296.
Luque de Castro, M., Priego-Capote, F., 2007. Ultrasound-assisted crystallization (sonocrystallization). Ultrason. Sonochem. 14, 717–724.
Matteucci, M., Hotze, M., Johnston, K., Williams III, R., 2006. Drug nanoparticles by antisolvent precipitation: mixing energy versus surfactant stabilization. Langmuir 22, 8951–8959.
Matteucci, M.E., Brettmann, B.K., Rogers, T.L., Elder, E.J., Williams III, R.O., Johnston, K.P., 2007. Design of potent amorphous drug nanoparticles for rapid generation of highly supersaturated media. Mol. Pharm. 4, 782–793.
Mersmann, A., 1999. Crystallization and precipitation. Chem. Eng. Sci. 38, 345–353.
Mosharraf, M., Nystorm, C., 1995. The effect of particle size and shape on the specific dissolution rate of micronized practically insoluble drugs. Int. J. Pharm. 122, 35–47.
Myerson, A., 2002. Handbook of Industrial Crystallization, second edition. John Wiley, New York.
Napper, D., 1970. Colloidal stability. Ind. Eng. Chem. Prod. Res. Dev. 9, 467–477.
Nishida, I., 2004. Precipitation of calcium carbonate by ultrasonic irradiation. Ultrason. Sonochem. 11, 423–428.
Noyes, A.A., Whitney, W.R., 1897. The rate of solution of solid substances in their own solutions. J. Am. Chem. Soc. 19, 930–934.
Patil, M., Gore, G., Pandit, A., 2008. Ultrasonically controlles particle size distribution of explosives: a safe method. Ultrason. Sonochem. 15, 177–187.
Prausnitz, J., Lichtenthaler, R., de Azevedo, E., 1999. Molecular Thermodynamics of Fluid Phase Equilibria, 3rd edition. Prentice Hall Inc., New Jersey.
Prozorov, T., Prozorov, R., Suslick, K., 2004. High velocity interparticle collisions driven by ultrasound. J. Am. Chem. Soc. 126, 1389–13891.
Raghavan, S., Trividic, A., Davis, A., Hadgraft, J., 2001. Crystallization of hydrocortisone acetate: influence of polymers. Int. J. Pharm. 212, 213–221.
Roelands, C.P.M., ter Horst, J.H., Kramer, H.J.M., Jansens, P.J., 2006. Analysis of nucleation rate measurements in precipitation processes. Crystal Growth Design 6, 1380–1392.
Ventosa, N., Veciana, J., Sala, S., Munto, M., Cano, M., Gimeno, M., 2005. New technologies for the preparation of micro- and nanostructured materials with potential applications in drug delivery and clinical diagnostics. Contribut. Sci. 3, 11–18.
Yeo, S.-D., Lee, J.-C., 2004. Crystallization of sulfamethizole using the supercritical and liquid antisolvent processes. J. Supercrit. Fluids 30, 315–324.
Zarkadas, D., Sirkar, K., 2006. Antisolvent crystallization in porous hollow fiber devices. Chem. Eng. Sci. 61, 5030–5048.
Zhao, H., Wang, J., Wang, Q., Chen, J., Yun, J., 2007. Controlled liquid antisolvent precipitation of hydrophobic pharmaceutical nanoparticles in a microchannel reactor. Ind. Eng. Chem. Res. 46, 8229–8235.